Optical Waveguide End Facet Roughness and Optical Coupling Loss

Hadi Baghsiahi, *Member, IEEE*, Kai Wang, *Member, IEEE*, Witold Kandulski, Richard C. A. Pitwon, and David R. Selviah, *Member, IEEE*

***Abstract*—This paper investigates the end facet roughness of multimode polymer channel waveguides fabricated on FR4 printed circuit boards, PCBs, when cut at right angles to their optical axis by milling routers for optical butt-coupling connectors and compares it with that resulting from dicing saws and polishing and proposes a novel end facet treatment. RMS surface roughness of waveguide end facets, measured by AFMs, are compared for a range of rotation speeds and translation speeds of a milling router. It was found that one-flute routers gave significantly less rough surfaces than two or three-flute routers. The best results were achieved for a one-flute router when the milling bit was inserted from the PCB side of the board with a rotation speed of 15,000 rpm and a translation speed of 0.25 m/min which minimized the waveguide core end facet RMS roughness to 183 ± 13 nm and gave input optical coupling loss of 1.7 dB ± 0.5 B and output optical coupling loss of 2.0 dB ± 0.7 dB. The lowest RMS roughness was obtained at chip loads of 16 μm/revolution. High rotation speeds should be avoided as smearing of the end facet occurs possibly due to polymer heating and softening. For the first time to our knowledge, channel waveguide optical insertion loss is shown to be linearly proportional to the ratio of the waveguide core end facet RMS roughness to its autocorrelation length. A new fabrication technique for cut waveguide end facet treatment is proposed and demonstrated which reduces the insertion loss by 2.60 dB ± 1.3 dB which is more than that achieved by the closest available index matching fluid which gave 2.23 dB ± 1.2 dB. The new fabrication method gives a more robust end facet for use in commercial products.**

***Index Terms*—AFM, atomic force microscope, channel waveguide, chip load, CNC tool, coupling loss, dicing saw, end facet roughness, fabrication, FR4, insertion loss, integration, manufacturing, micromechanical, milling router, multimode waveguide, Nomarski microscope, optical attenuation, optical circuit board, optical coupling, optical printed circuit board, optical waveguide, packaging, PCB, polymer waveguide, roughness analysis, router bits, router tool.**

Manuscript received April 15, 2013; revised June 24, 2013; accepted June 25, 2013. Date of current version July 17, 2013. This work was supported by UK Engineering and Physical Sciences Research Council (EPSRC) via the Innovative electronics Manufacturing Research Centre (I eMRC) Flagship Project: Integrated Optical and Electronic Interconnect PCB Manufacturing (OPCB) FS/06/01/01 project grant, by Dorothy Hodgkin Postgraduate Award support for H. Baghsiahi, and by direct industrial help from Stevenage Circuits Ltd.

H. Baghsiahi and D. R. Selviah are with the Department of Electronic and Electrical Engineering, University College London (UCL), London, WC1E 7JE, U.K. (e-mail: h.baghsiahi@ee.ucl.ac.uk; d.selviah@ucl.ac.uk).

R. C. A. Pitwon and K. Wang are with Xyratex, Havant, Hampshire PO9 1SA, U.K. (e-mail: Richard_Pitwon@xyratex.com; kai_wang@xyratex.com).

W. Kandulski was with Stevenage Circuits Limited, and is now with UTC Aerospace Systems (e-mail: wkandulski@googlemail.com).

Color versions of one or more of the figures in this paper are available online at http://ieeexplore.ieee.org.

Digital Object Identifier 10.1109/JLT.2013.2271952

I. Introduction

ADVANCED computers, supercomputers, storage arrays, switching fabrics and measurement instruments often use a rack chassis configuration. In this arrangement, multiple daughter boards, mezzanine boards, blade servers, controllers, drive cards or power supplies on which active components are mounted and interconnected, are plugged in at right angles to a continuous backplane, mid-plane or motherboard which extends from one side of the chassis to the other [5] and which has the important function of interconnecting the daughter cards. As a result, the highest data traffic occurs on the backplane and at bit rates exceeding about 10 Gb/s the interconnect technology of multiple levels of copper tracks within a printed circuit board, PCB, suffers from signal loss, distortion, crosstalk and EMI [1]. A commercially attractive solution is to also embed optical interconnects into the PCB backplane [1] in the PCB manufacturing company using their existing fabrication equipment. Optical interconnects are scalable to much higher bit rates as demonstrated in optical fibre communication. However, in order for the highest speed copper tracks to be replaced by optical interconnects the full technology of optical interconnects must be of a similar low cost. Optical circuit boards have been demonstrated using layers of overlapping optical fibres glued onto the PCB or glued together into a film which can be applied to the PCB [2], however, optical waveguide technology offers a lower cost approach that can be fabricated using existing technology used to fabricate PCBs [3]. Low cost optical connectors are required to connect the optical backplane waveguides to optical components on the daughter boards such as lasers and photodiodes. There are two approaches to make a connector. In one approach, the waveguide ends in a 45-degree mirror tilting the beam normal to the surface but this requires more complex and costly fabrication procedures in order to obtain low loss 45-degree mirrors [4].

In a simpler, lower cost approach, the waveguide end is cut at right angles to its optical axis to form a flat end facet and VCSEL lasers are directly butted up against the facet. In practice, lenses are usually used to image the laser onto the waveguide facet and at the other end lenses image the output waveguide facet onto the photodiode [5]. This protects the face of the laser and photodiode and avoids knocking off any bond wires attached to the active optical components during mating. Low cost, passively aligned optical connectors have been reported [6], incorporating

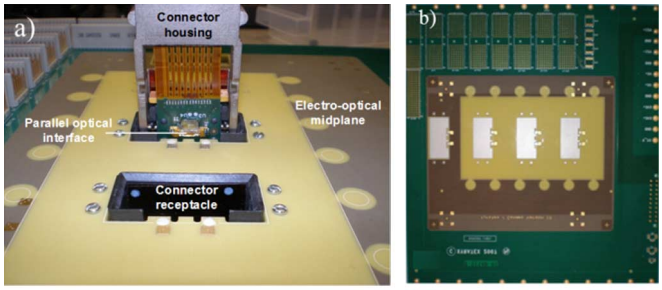

(a) (b)

Fig. 1. Electro-Optical Circuit Board backplane having multiple layers of copper tracks, and vias with one optical waveguide interconnect layer on the surface. The 4 white apertures in the board shown in part (b) are cut out using a router and are where the daughterboards are connected to the backplane (a).

such active components, which allow repeated insertion and disengagement of the daughter boards and yet still maintain highly accurate alignment of the VCSEL laser arrays and PIN photodiode arrays mounted on the daughter boards with the waveguides and associated lenses mounted on the backplane.

One approach for connector-waveguide coupling is to arrange for all of the connectors to be located around the edges of a rectangular optical circuit board [7] but this limits the flexibility of layout arrangements. For most flexibility and compatibility with current designs of chassis-rack based instruments, apertures must be cut out of the PCB, Fig. 1, to allow access to the arrays of lasers and photodiodes [8]. For waveguides ending at the edge of a board the edge can be cut using a dicing saw similar to those used to cut silicon wafers into chips, and to give good optical coupling, the edge can be polished to reduce any roughness. However, when the waveguide ends in a milled aperture in the board, it is not known how rough the resulting waveguide end facet is nor how it may be polished or smoothed, nor how much optical loss is incurred when coupling in or out of these waveguide facets and it is the aim of this paper to address these issues.

Various other methods have been investigated for cutting optical printed circuit boards, OPCBs, sometimes called optical circuit boards, OCBs, such as using, laser ablation or chemical etching.

For laser cutting or ablation, it has previously been shown [8], [9] that it is necessary to precisely control the laser characteristics, collimation, pulse repetition rate, beam size and power distribution profile to achieve smooth cuts through several layers of different material. The laser beam must also be precisely aligned to the workpiece and the beam shaping and power control optics adjusted to cut through the different layers which comprise two different polymers, FR4 and a copper layer [8], [9]. Chemical etching, plasma etching, sand blasting, blade cutting or stamping with a shaped blade are not suitable for this application due to the cost and damage that can be involved with these methods.

This paper is concerned with the use of a milling router as a practical production line technique, which is already readily available in PCB manufacturers, to cut the waveguide ends. This has the advantages that it is easy to use and control CNC machines and a wide range of sizes of cuts and shapes are possible without damage to other parts of the OPCB. Milling routers have already been used for cutting polymer waveguides [10], [11]. However, the surface profile left after milling polymer waveguides has not been previously studied in depth nor its relationship to the effect on optical input and output coupling loss although earlier researchers have noted that it is essential to have this information [12].

When a laser beam with a certain divergence angle impinges on a rough waveguide end facet the light is scattered both forwards and backwards over a wider divergence angle than that in the original beam [13]. The divergence angle and polar scattering diagram can be found by calculating the two-dimensional Fourier Transform of the roughness profile assuming uniform intensity and plane wave illumination. This assumption may be valid for laser illuminated waveguide inputs for collimated laser beams but breaks down at the waveguide exit where the modes interfere to give an almost random phase distribution and speckle. The strength of the scattered light depends on the root mean square (RMS) value of the roughness, σ, [14]. The divergence angle of the scattered light depends on the inverse of the autocorrelation length, T, of the roughness [15] which is a measure of the fineness of the roughness. Therefore, it is helpful to define a figure of merit, σ/T which combines both contributions to the input and output optical coupling loss [16], [17].

In this paper, the effect of milling routers on the end facet roughness of polyacrylate waveguides on FR4 PCBs is presented in Section II together with a thorough analysis. In Section III, the relationship between the optical loss and the end facet roughness of the polyacrylate waveguides on FR4 PCBs is experimentally established for the first time and in Section IV, a new method for reducing the waveguide end facet roughness, and so the optical coupling loss, is devised and successfully demonstrated.

II. Waveguide End Facet Cutting Methods

A. Waveguide Core End Facet Roughness When Cut With a Milling Router

The end facet roughness of waveguides cut using a variety of types of milling router tools was investigated. Three different routers with different numbers of cutting edges (called flutes) were chosen to find the router which leaves the end facet with the smoothest surface. Multimode waveguides were manufactured photolithographically from Truemode® Acrylate based polymer on the surface of FR4 PCB, which had their other surface coated in a typical layer of 50 micron thick copper, in Exxelis Ltd, a polymer manufacturer, and were cut in Stevenage Circuits Ltd, which is a PCB manufacturing company, to give realistic results of what might be achieved in a commercial production line process.

The routers were made of silicon carbide and had a diameter of 1.6 mm and blade angle of 45° were supplied by Ernst Wessel Machinebau Gmbh. The routers were mounted in a CNC milling machine which was used to perform the various waveguide cuts (Fig. 2).

Some experiments were initially carried out to establish the best orientation for the waveguide on PCB samples in the CNC machine. In one orientation, the waveguide (upper cladding) was uppermost and in the other orientation the copper/FR4 was uppermost.

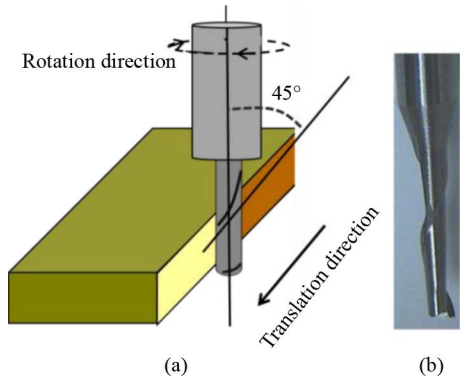

Fig. 2. (a) Schematic diagram of a one-flute router and the cutting procedure used for the roughness investigation. (b) A one-flute router (RLG 615) from Ernst Wessel Machinebau Gmbh.

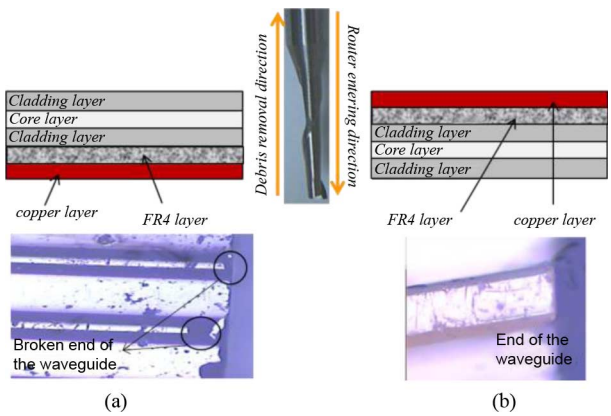

Fig. 3. Photomicrograph of the end of the waveguide after cutting with a one-flute router entering the sample from (a) the waveguide and (b) the copper coated FR4 PCB side. For scale the waveguides are 50 microns wide.

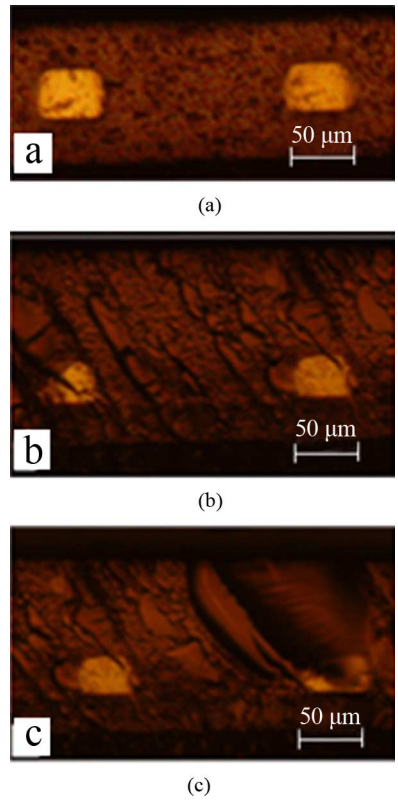

Fig. 4. Photomicrographs of cross section end facets of polymer multimode waveguides cut by (a) one-flute router cutter ($\sigma = 183$ nm, $T = 2.6$ μm), (b) two-flute cutter ($\sigma = 540$ nm, $T = 4.3$ μm), (c) Three-flute cutter ($\sigma = 911$ nm, $T = 6.6$ μm). The waveguides were cut with the same rotation (15000 rpm) and translation speed (0.25 m/min) for a valid comparison.

The photomicrographs in Fig. 3 show a plan view of the end of the waveguide after cutting. When the router is inserted from the waveguide side, Fig. 3(a), the end of the waveguide breaks. In this orientation, Fig. 3(a), there is just one layer, namely the cladding, on top of the waveguide core material and rotating the router pulls the layers upwards and away from the PCB, possibly causing some delamination, resulting in a broken waveguide end. However, when the router is inserted from the copper-coated FR4 PCB side, Fig. 3(b), the rotation creates a force which pulls the waveguide core towards the thicker copper/PCB/cladding which serves to support it. The milling experiments were repeated using a PCB without a copper layer and it was found that it is better to remove the copper layer at the location of the cutting before milling the sample to avoid copper dust embedding in and contaminating the end of the waveguide. The copper layer was removed by surface milling. However, it was found that even if the copper is not removed, the copper dust contamination of the end facet is less when the waveguide is facing downwards as the copper dust is moved upwards away from the waveguide core material in this orientation.

Further experiments were carried out to assess the effect of the number of cutter flutes on the waveguide end facet surface finish. The shape of the router and the numbers of flutes on the router had previously been reported to have an effect on the surface roughness of other surfaces such as metals or plastics when cut by a milling machine [10]. Three milling router cutters with different numbers of flutes with the same flute properties (material, flute angle, flute direction) were chosen and used to cut the waveguide samples. The router tips were new and unused. Several similar router tips were used to make sure that a surface roughness was not due to a particular damaged or poorly made router. Fig. 4 shows the waveguide end surface cross sections cut using routers having differing numbers of flutes. The photomicrographs were taken through a Nomarski microscope with the waveguides back-illuminated using white light. The yellow part is the core material of the waveguide surrounded by the cladding material, which appears brown.

The end facet roughness was measured using an Atomic Force Microscope, AFM (Veeco Dimension 3100V, 7 nm tip radius), and analyzed using in-house software to determine the root mean square, RMS, roughness in nanometers across the 30 micron by 30 micron area of the scan over the waveguide core and to determine the 1D autocorrelation length, T, along the direction parallel to the surface of the PCB. A number of other measures of surface roughness such as peak to peak roughness, R_{t}, maximum surface height, R_{p}, minimum surface height, R_{v}, skewness, R_{sk}, kurtosis, R_{ku}, and arithmetic average of absolute values, R_{a}, were also calculated [18] but it was found that the RMS roughness, σ, or R_{q}, gave more reproducible results so only RMS roughness is used in this paper. The three-flute router cutter gives a very rough surface (RMS roughness, σ of 911 ± 285 nm). Some groove or gouge-shape structures,

TABLE I
RMS SURFACE ROUGHNESS AND CHIP LOADS OF WAVEGUIDE CORE END FACETS CUT USING A ONE-FLUTE ROUTER FOR A RANGE OF ROTATION AND TRANSLATION SPEEDS

Rotation speed (rpm) → / ↓Translation Speed (m/min)		5000	15000	34000	50000
0.10	Roughness (nm)	389 ± 61	310 ± 12	384 ± 10	342 ± 23
	Chip load (μm/revolution)	20	6.6	2.9	2
0.25	Roughness (nm)	376 ± 30	183 ± 13	358 ± 12	339 ± 42
	Chip load (μm/revolution)	50	16	7.4	5
0.50	Roughness (nm)	474 ± 32	381 ± 18	205 ± 24	410 ± 15
	Chip load (μm/revolution)	100	33	15	10
0.75	Roughness (nm)	434 ± 54	386 ± 20	407 ± 43	296 ± 12
	Chip load (μm/revolution)	150	50	22	14

Fig. 4(c), could be observed on the cross sectional surface cut by the three-flute cutter. Diagonal grooves at an angle of $40° \pm 5°$ to the PCB surface remain on the waveguide end facet, Figs. 4(b) and 4(c) after cutting with either the two-flute or three-flute routers. Fig. 4(a) shows that the one-flute cutter gives the best and smoothest surface (RMS roughness, σ of 183 ± 13 nm). Only some slight traces of diagonal grooves at an angle of $40° \pm 5°$ to the PCB surface can just be discerned.

B. Waveguide Core End Facet RMS Roughness as a Function of Router Rotation and Translation Speed

As the one-flute router gave the best cross sectional surface finish this was chosen for the following optimization experiments to find the best rotation and translation speeds to minimize the waveguide end facet surface roughness. Several rotation and translation speeds were used. As before the waveguides were cut by a commercial PCB manufacturer, Stevenage Circuits Ltd using their CNC milling machine (Wessel CNC MLB2 Drill/Router) to simulate the fabrication and cutting of the waveguide end facets in a realistic industrial environment. Table I shows the RMS roughness of polymer waveguide end facet surfaces measured over an area of 30 microns by 30 microns of the waveguide core cut at a variety of rotation and translation speeds. To estimate the measurement accuracy, typically three or four areas across the waveguide core cross section were scanned by the AFM and for each area the RMS roughness was calculated. Then the standard deviation between these RMS values for different scan areas was taken as the measurement accuracy.

Fig. 5 shows a contour plot of the waveguide core end facet RMS roughness data of Table I. The minimum roughness region, in blue (dark) color appears as a diagonal valley across the middle of the plot. This means that to achieve a surface with a lower magnitude of RMS roughness, the translation speed and rotation speed should be set at the minimum of the valley and

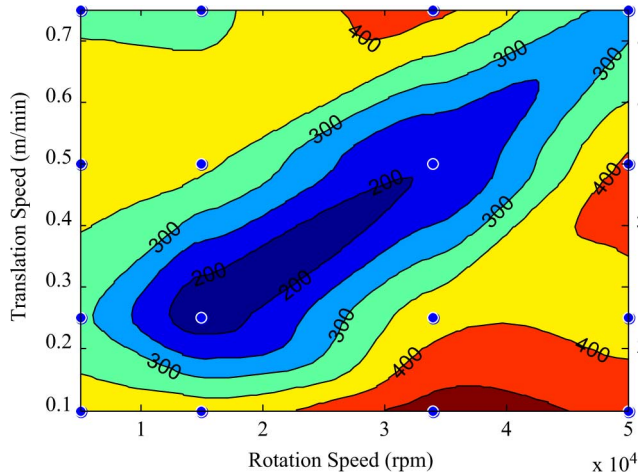

Fig. 5. Waveguide Core End facet RMS roughness plotted as a contour plot as a function of router rotation and translation speed. The units of roughness on the contour labels is nm. The blue dots indicate the data points between which the graph has been interpolated.

increased or decreased together to remain within the low part of the valley. So, small rotation speeds should be used with small translation speeds and vice versa. High translation speeds and high rotation speeds will remove material faster. However, according to Table I and Fig. 5 the RMS roughness is minimized for lower translation and rotation speed combinations.

C. Surface Finish of Waveguides Cut With a One-Flute Router at High Rotation Speeds

If the translation speed is slow and the rotation speed is high then any part of the surface will be touched many times as the router rotates which may give a polishing action and will certainly heat the surface up due to friction possibly softening the polymer. If the rotation speed is low and the translation speed is high then any point of the surface may receive less polishing and heating. In selecting the optimum combination of translation and rotation speeds, it is not sufficient simply to examine the RMS roughness of the waveguide core end facet but it is also important to view this surface through a microscope.

Fig. 6 shows the end facet of a waveguide cut at a rotation speed of 34,000 rpm and a translation speed of 0.75 m/min with the waveguides back illuminated using white light. The waveguide surface appears blurred although the Nomarski microscope is focused on surrounding regions of the surface. When the microscope is moved towards and away from the surface the waveguide cannot be brought into focus so the waveguide core is not cut back by more or less than the surrounding material.

For comparison, Fig. 4(a) shows similar waveguides but cut at a much slower rotation speed of 15,000 rpm and a much slower translation speed of 0.25 m/min and shows the core in focus very clearly. Therefore, it may be that the core and cladding have softened due to heating and have been smeared across one another in the high rotation and translation speed case. When the rotation speed is increased to 60,000 rpm and 70,000 rpm, similar apparently smeared layers across the waveguide core area also observed. The samples shown in Fig. 6 were cleaned by blowing a jet of air across the surface

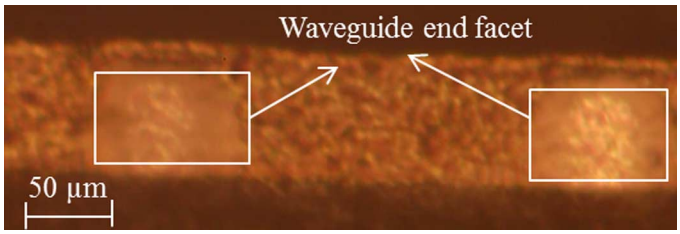

Fig. 6. Photomicrograph taken through a Nomarski microscope of a back illuminated waveguide cut at a rotation speed of 34,000 rpm and a translation speed of 0.75 m/min.

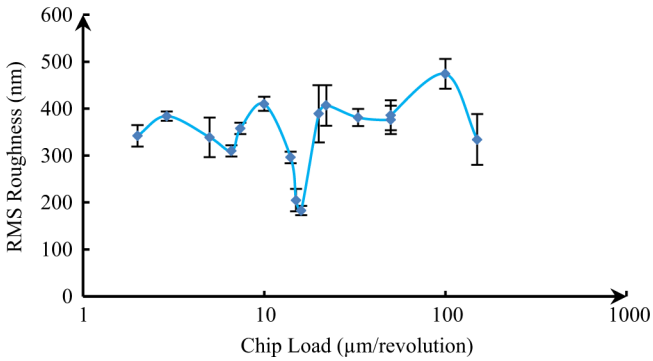

Fig. 7. RMS roughness of the waveguide core end facet after cutting with a one-flute router as a function of chip load in units of microns per revolution of the router.

but the images did not change so it cannot just be dust or small swarf particles.

III. Waveguide End Facet Roughness Analysis

A. Chip Load Analysis

The concept of chip load is used in the milling industry so it is important to re-express the earlier findings in terms of chip load. Chip load is defined as the ratio of the translation/(rotation speed in rpm$\times$number of flutes) [19]. Chip load units are expressed in microns per rotation of the router in this paper. Chip load combines both the rotation and translation speeds into a single variable which is an indication of how much material is removed per rotation and distance traversed by the router. Router tool manufacturers recommended for these routers to start with a chip load of $8\ \mu\mathrm{m}$ revolution and to vary the rotation and translation speeds to optimize the surface finish. The chip load was calculated and is tabulated in Table I and is plotted in Fig. 7 as a graph of waveguide core end facet roughness versus chip load. In Table I it is clear that similar chip load values tend to lie along diagonals across the table in a similar direction to the diagonal of the lowest RMS roughness values.

Fig. 7 shows a minimum RMS roughness, larger than oscillations due to experimental error, at a chip load of $16\ \mu\mathrm{m}$ revolution. The RMS roughness at the minimum is $183 \pm 13\ \mathrm{nm}$. A number of data points are recorded in Table I and these are all consistent with an interpolated single large minimum valley in Fig. 5 which corresponds with the minimum in Fig. 7. Our trials did not show any other minima.

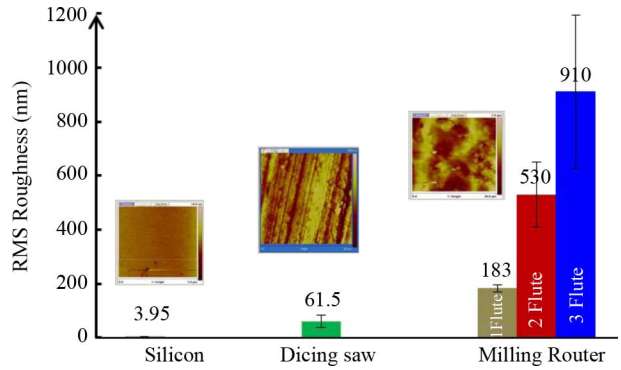

Fig. 8. RMS Roughness of the waveguide core end facet surfaces of waveguides cut using routers with different number of cutting edges or flutes and by a dicing saw in comparison to a silicon wafer surface. An AFM image is shown for each surface for comparison of the surface profile. The number on top of each bar is the RMS roughness in nm for that sample.

B. Comparison of Waveguide Cutting Methods

Traditionally waveguides are cut using a dicing saw consisting of a disc impregnated with particular types and sizes of grit so it is necessary to compare the surfaces cut by the routers with similar waveguides cut using a dicing saw. The scope of this research was insufficient to investigate a variety of types and sizes of grit on the dicing saw and translation and rotation speeds so a typical dicing saw with silicon carbide grit of size $30\ \mu\mathrm{m}$ used for cutting PCBs at the London Centre of Nanotechnology (LCN) at their standard rotation speed of 30,000 rpm and translation speed of 0.6 m/min was used. Fig. 8 gives an overview of the comparison of RMS roughness of the waveguide core end facet after cutting with a three-flute router, a two-flute router, a one-flute router at the optimum rotation and translation speeds for minimum roughness, a dicing saw and a silicon wafer. The roughness of a silicon wafer was considered as an ideal smooth surface for comparison purposes to assess the measurement accuracy of the AFM.

Fig. 8 shows that, although the waveguide core end facet roughness for the one-flute router at optimized rotation and translation speeds is somewhat less than that of the two-flute and three-flute routers, it is still at $183 \pm 13\ \mathrm{nm}$, more than double that for a similar waveguide sample cut by a dicing saw which had a surface roughness of $61.5 \pm 23\ \mathrm{nm}$. However, it is interesting that the error bar for the surface milled by the one-flute router is less than that due to the dicing saw showing more reproducibility between cut samples which is of importance for manufacturing on production lines. The silicon wafer, of course, had the best surface RMS roughness of $3.95 \pm 2\ \mathrm{nm}$.

C. Spatial Roughness Uniformity

As shown earlier it is not sufficient to just consider RMS roughness in isolation. Fig. 9 shows another aspect of the roughness; which is the way the roughness changes across a sample and compares this for the same samples measured in Fig. 8. To calculate the data for Fig. 9, an area of $30\ \mu\mathrm{m} \times 30\ \mu\mathrm{m}$ of the waveguide core end facet on each sample was scanned and the result was saved in a 256×256 array of raw roughness data

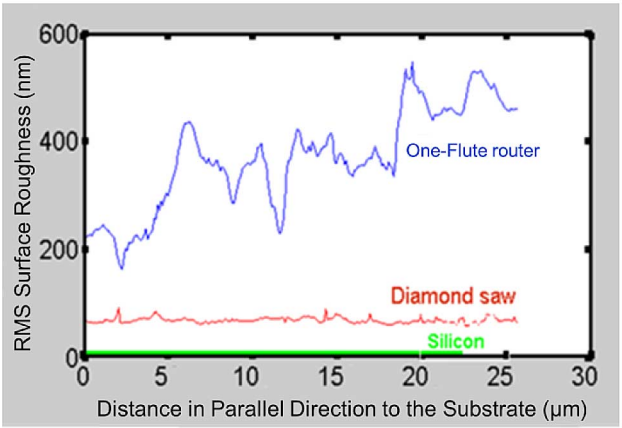

Fig. 9. The spatial variation of 1D surface RMS roughness for waveguide core end facets cut using a one-flute router with 34000 rpm and 0.75 m/min translation speeds, a dicing saw and a comparison with a silicon wafer.

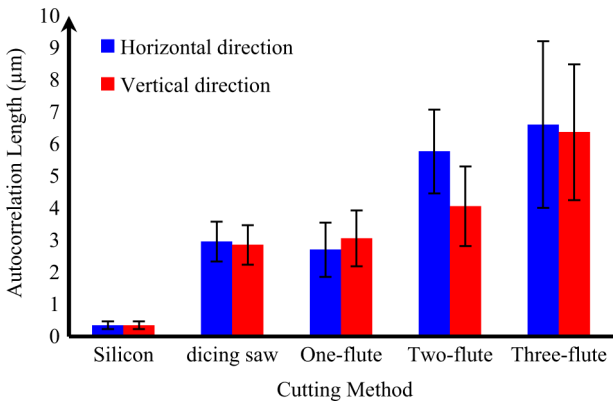

Fig. 10. Autocorrelation length of the samples cut with different methods.

values. The RMS roughness of each column parallel to the substrate was then calculated and plotted in Fig. 9.

Although the one-flute router at optimum rotation and translation speeds across a 2D area of several samples gave an RMS roughness of 183 ± 13 nm, for a single poor sample shown in Fig. 10 at un-optimized rotation and translation speeds, the RMS roughness is not consistent across the sample and can reach substantially higher values. The dicing saw gave much more consistent results across the sample.

D. Autocorrelation of the Roughness

Apart from RMS roughness magnitude and uniformity, the scattering properties of light incident on a waveguide end facet are also influenced by whether the roughness is coarse or fine. This can be quantified by calculating the autocorrelation length of the roughness which is taken to be the distance from the vertical axis to the curve at 1/e of the peak value of the autocorrelation function at the origin [15].

A small autocorrelation length indicates that the roughness is fine and has a short period resulting in optical scattering into large angles. This means that more light is coupled into higher order bound propagating modes and beyond them into unbound radiation modes [20] resulting in more input coupling loss. The

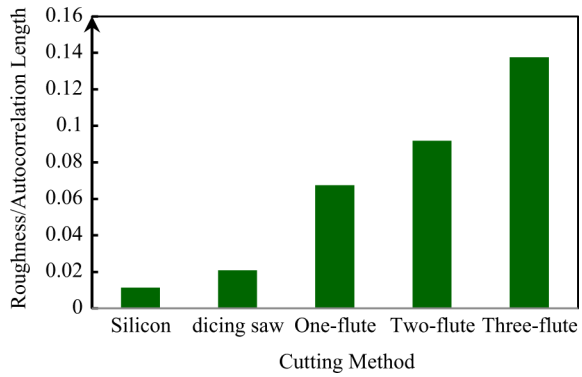

Fig. 11. Ratio of σ/T for different cutting methods.

higher order bound modes interact with waveguide sidewall roughness [20] resulting in higher propagation loss. Also at the input to the waveguide the roughness causes backscattering over similar large angles resulting in increased input coupling loss. At the output from the waveguide a small autocorrelation length results in wide angle scattering requiring high numerical aperture optics if output coupling loss is to be avoided. Similarly, a larger magnitude of RMS roughness results in more optical loss. Therefore, it is useful to combine these together in a single figure of merit as the ratio of RMS roughness to autocorrelation length, σ/T, so that increased values of this figure of merit either due to increased RMS roughness or decreased autocorrelation length, result in increased optical coupling loss. Fig. 10 shows the autocorrelation length of waveguide core end facet roughness samples cut by different methods. The autocorrelation length was calculated separately in the horizontal and vertical scan directions. Fig. 11 shows the ratio of RMS roughness to autocorrelation length, σ/T, for waveguide core end facet roughness samples cut by different methods.

Fig. 10 shows that the autocorrelation length in the horizontal and vertical directions are the same to within experimental error apart from for the 2-flute router. Perhaps a difference would appear if this were calculated along the grooves and normal to the grooves seen in Fig. 4. The AFM trace of the three-flute router was not continuous due to severe surface steps so the autocorrelation calculations for that case may not be completely valid. Fig. 11 also shows that the autocorrelation length of the sample cut by the dicing saw is the same as the sample cut using a one-flute router at its optimized rotation and translation speed to within experimental error. However, by comparing photomicrographs of the waveguide core end facet cut by the one-flute router using optimized speeds with that due to cutting with the dicing saw (Fig. 8), it is apparent that the dicing saw leaves more periodic grooves due to the grit particles embedded in the saw blade. Periodic grooves result in two equally angled scattered beams due to the Fourier Transform relationship between the far field and near field profiles. Therefore, at the input waveguide facet it would excite certain modes preferentially.

Fig. 11 shows that the figure of merit, σ/T is lower for the dicing saw than for even the one-flute router at optimised speeds. Smaller values of, σ/T indicate reduced expected optical coupling loss.

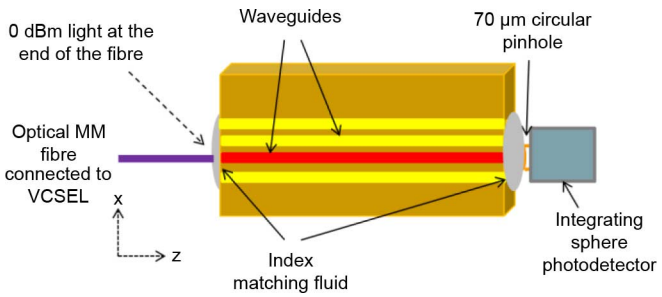

Fig. 12. Experimental configuration for waveguide optical loss measurements. One 850 nm VCSEL was connected to a $50/125\mu$m MM fibre via an ST connector and was set to provide an output optical power of 0 dBm at the output end of the fibre.

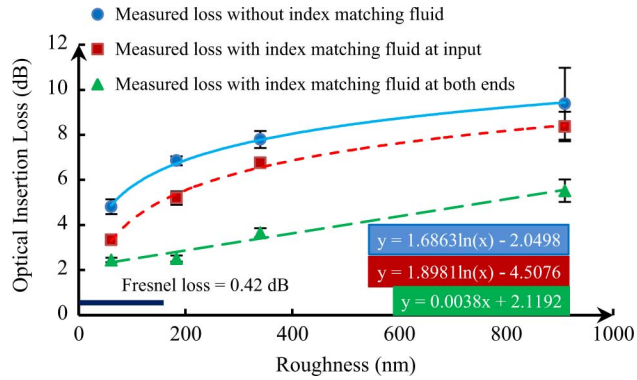

Fig. 13. Experimental results for the optical insertion loss of a set of waveguides.

IV. Waveguide End Facet Roughness and Optical Loss

A. Optical Insertion Loss, Input and Output Coupling Loss Due to the Roughness of the Waveguide Core End Facets

Although the figure of merit, σ/T should give an indication of the optical coupling loss, for precision and confidence it is necessary to measure the optical input and output coupling losses as a function of waveguide core end facet roughness and cutting method. Identical waveguide samples with different magnitudes of waveguide core end facet roughness were scanned by AFM and then the optical loss was measured by experiment. A multimode fibre coupled VCSEL with 850 nm centre wavelength was used as the source $(\mathrm{NA} = 0.22)$. The receiver was a photodetector, PD, with an aperture of 70 μm (PD). The experimental method is shown in Fig. 12 and described in [5] to calculate the overall attenuation or insertion loss.

In some of the experiments, one and then the other end facet of the waveguide was coated in an oil with a similar refractive index as the waveguide core. The index matching fluid penetrates between the microstructure of the roughness and fills the space removing the effect of the optical scattering due to the roughness. This enables the effect of the roughness to be quantified. The closest available index matching fluid had a refractive index of $n = 1.5694 \pm 0.0005$ at 840 nm wavelength, and was supplied by Cargille Laboratories (code: LCABK)). The data of the refractive index of the oil at 850 nm was not available. The polymer core refractive index was $n = 1.5560$ at 850 nm wavelength so it was a close but not a perfect match. It was used in turn to fill the source to waveguide and then the waveguide to PD interfaces to reduce the coupling loss.

Fig. 13 shows the experimental results of optical insertion loss for a set of waveguide samples with different magnitudes of roughness cut by differing means. The optical insertion loss includes the input coupling loss, the propagation loss and the output coupling loss. The waveguides were all fabricated at the same time by the same process and were all cut to the same length of 1 cm so the propagation loss should be the same for each. Each experimental point is the average of 10 measurements on different samples together with an error bar which is the standard deviation between those sample results.

Generally as the RMS roughness increases the loss increases. For the untreated waveguides, the insertion loss reduces from the three to the two to the one-flute router to the dicing saw

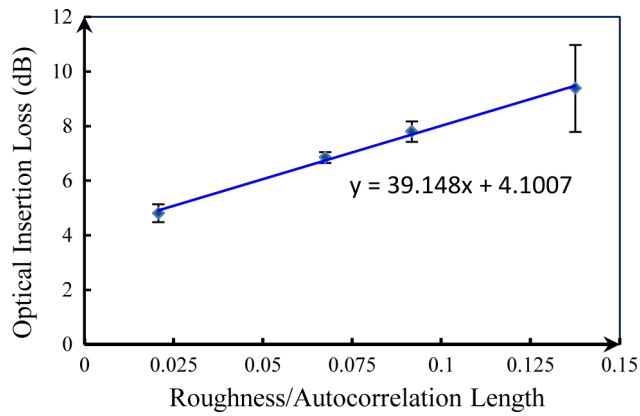

Fig. 14. Optical insertion loss plotted versus, σ/T ratio of RMS roughness to autocorrelation length of the waveguide core end facet roughness.

as each roughness point in Fig. 14 was caused by these cutting methods in turn from right to left. This trend agrees with the trend in the figure of merit, σ/T for the same cutting methods, by comparing Figs. 14 and 11. One would expect that as the roughness tends to zero all of the curves in Fig. 13 should tend to the same value of the Fresnel Loss, 0.42 dB for both ends together, as calculated from the core refractive index, $n = 1.5560$, plus the propagation loss 0.08 dB/cm giving an overall insertion loss of 0.50 dB. However, this does not seem to be the case as the curves tend towards about 2 dB giving an extra 1.5 dB unaccounted loss. This additional loss is partially due to the shadowing due to the combination of a pinhole and PD, which not only cuts out any radiation modes travelling in the cladding but also some light diverging from the $50\ \mu\mathrm{m} \times 50\ \mu\mathrm{m}$ square waveguide core. Moreover, the index matching fluid was not a perfect match and the analysis of Section IV B suggests that this results in an additional 0.37 dB loss. When index matching fluid is applied, the loss reduces for all magnitudes of roughness.

Fig. 14 shows the optical insertion loss of the waveguides plotted versus the figure of merit, σ/T. This clearly shows a very good linear relationship. Fig. 14 showed that optical insertion loss is not directly proportional to waveguide core end facet roughness, however, Fig. 14 shows that optical insertion loss is linearly related to the figure of merit, σ/T, showing the importance of including the autocorrelation length, T, in the figure of merit. This is an important result and is true irrespective of the

method of cutting as each point in Fig. 14 represents a different method of cutting the waveguide end facet. This graph also shows how much the end facet must be polished or smoothed in order to reduce the insertion loss by a specified amount. However, if this straight line is extended to cut the vertical axis the insertion loss value is not the 2 dB expected from Fig. 13. So we conclude that this linear relationship must break down for smaller values of the figure of merit, σ/T

B. Waveguide End Facet Roughness Treatment Using a Layer of Cured Polymer

In the previous section, it was shown that the application of refractive index matching fluid at the input and output waveguide facets reduces the insertion loss, Fig. 13, by 2 dB for a dicing saw cut and 2.6 dB for a one-flute router with optimized speed cut. However, refractive index matching fluid is not an ideal solution for reducing the effect of the roughness of waveguide facets. Over time, the index matching fluid evaporates gradually resulting in increased insertion loss. The insertion loss of waveguide samples with 61 nm and 910 nm RMS roughness increased to 3.9 dB and 8.1 dB two days after applying index matching fluid at both ends of the waveguides, which is approaching their original values on Fig. 13 before application of index matching fluid. The index matching fluid may contaminate other parts of the board and must be continually replenished which is not practical. The liquid also collects dust over time. Therefore, a more durable method is required as index fluid matching is just a temporary solution to reduce loss.

The waveguide samples cut by the milling router and dicing saw were also polished in order to examine its effect and to determine the challenges of manual polishing. Three types of silicon carbide grinding paper were used from coarse to fine grain. Polishing was carried out using a sequence of operations with progressively finer grains, these were, 20 μm grit sand cloth, 3 μm aluminum oxide polishing cloth, 1 μm fine grit aluminum oxide polishing cloth. Cerium oxide 'Jewellers' Rouge' could also have been used in which the grain size reduces with use giving a progressively finer surface structure. The samples were rubbed on the surface of polishing paper in a figure of eight-shaped path when the polishing paper was held in a fixed position. Two people operated on each sample in two minute sessions with 1-2 sessions for smoothing and 2-4 sessions for polishing. Each sample was held perpendicularly to a sanding table mounted and fixed on the floor. The sample was flipped 180° around the vertical axis every 5-6 seconds to minimize polishing error caused by sample orientation and rotation speed of the hand. This type of error results in the surface not being flat but instead being tilted at different angles with deviations up to a few degrees to the horizontal direction. This is due to the sample being tilted during polishing or can be due to the differing hardness of different materials such as FR4 and polymer. A jig could have been used to maintain the waveguides at right angles to polishing paper. Nevertheless, hand polishing is not a reliable method of reducing roughness as the finished surface quality is dependent on the ability of the polishing operative, the force applied and other human factors. Moreover, it is not suitable for mass production as a mechanical arm is needed to do the polishing which increases the cost and the results are inconsistent for a given type of board for several reasons. Firstly, the copper layer must be removed otherwise there will be a lot of copper dust contamination on the waveguide surface. Secondly, and more importantly, polishing removes some of the waveguide material so the polished end facet of the waveguide will not be exactly where it was cut, thus, increasing the gap between the laser source and the waveguide or the waveguide and the photodetector if the alignment method assumes the end surface to be at the cut position. Any gap results in increased coupling loss and increasing laser beam diameter due to divergence unless the amount of material polished away is taken into account so that the optical source is moved that much closer to the waveguide to compensate.

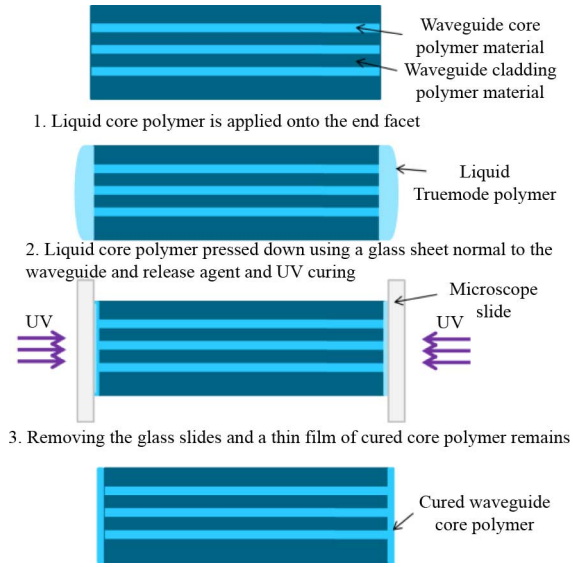

Fig. 15. New technique for coating the ends of an array of cut waveguides with core polymer and curing to leave a flat smooth surface.

Therefore, a new technique was developed to smooth the end facets of the cut waveguide. In this method, uncured liquid waveguide core material is coated on each of the end facets of the waveguide and cured to reduce the effect of end facet roughness. This actually acts like refractive index matching fluid without its drawbacks. The fabrication procedure is shown in Fig. 15. Firstly, a small amount of liquid waveguide core polymer is applied using a dropper onto one end of the waveguide core when the waveguide is held vertically. Actually, the polymer droplet also covers the cladding too in the experiment reported here without observable detrimental effects. Secondly, a release agent, Silicone Lubricant Aerosol (CP1051, CRC Industries UK Ltd) is spayed on one side of a glass microscope slide (made by Menzel-Glaser) and this coated microscope slide is pushed against the waveguide end facet to flatten and spread uniformly the liquid core polymer droplet. Care was taken to make sure the waveguide was held perpendicular to the microscope slide. A clamp was used to apply force to the microscope slide of approximately 1.3 kPa which gave a layer

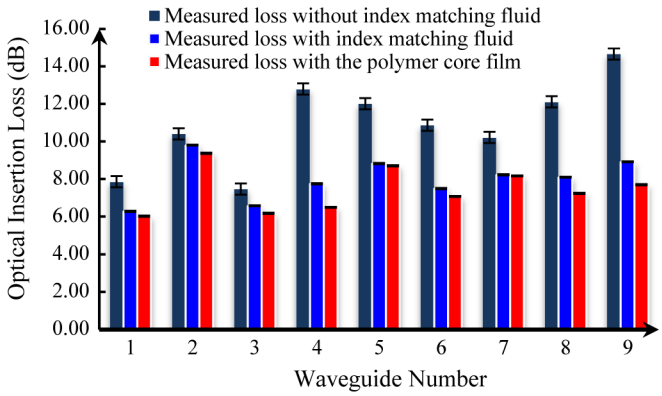

Fig. 16. The insertion loss of a range of 9 waveguides with the same RMS roughness. The improvement of the coupling loss after applying index fluid matching on average is 2.23 ± 1.2 and after applying Truemode ™ acrylate polymer is 2.60 ± 1.3. There is an error bar on each column in the figure.

thickness of $10 \pm 2\ \mu\mathrm{m}$. It may be better to use a flatter surface such as an optical interferometer mirror with $\lambda/20$ or $\lambda/40$ or better but in the experiment reported a microscope slide was used. The surface roughness of the microscope slide was 9 ± 3 nm (measured by AFM) about twice as much as a silicon wafer. This was used to achieve a flat surface at the end of the waveguide and to be transparent to allow Ultraviolet, UV, light to pass through it to cure the polymer.

UV light was then used to cure the polymer through the glass slide and the glass slide was removed. The result was a flat surface as smooth as the microscope slide. Both end facets were treated in the same manner. In this paper, we report its use when applied to nine waveguides terminating in a mid-board aperture for a commercial optical interconnection demonstrator. The waveguides had different lengths [5] and different numbers of bends and crossings.

In the intended application [5] a VCSEL is directly imaged onto the end facet of the waveguide. The addition of an extra core layer causes an apparent depth phenomenon resulting in a slightly different focal z position which can be taken into account in the design of the connector.

The nine waveguides were measured before and after applying refractive index matching fluid and before and after applying core polymer and curing it according to the procedure described. All of the waveguides were cut with the same milling router and had similar roughness profiles. The optical loss measurement procedure was similar to that shown in Fig. 12 except that the PD was a photodiode with a smaller form factor to fit inside the apertures [5]. The launch conditions were as follows: An ST connector packaged 850 nm VCSEL was connected to a standard $50/125\ \mu\mathrm{m}$ step-index multimode (MM) fiber with NA_{fiber} of 0.22. The fiber was 10 m long and was wound 20 times around a 38 mm diameter cylindrical mandrel in order to fill the *NA* of the fiber and we confirmed [5] through measurement that the *NA* of the fiber was fully filled with a large number of transverse modes. The results for insertion loss are shown in Fig. 16 where the waveguide number is arbitrary but relates to the same number as in [5].

Fig. 16 shows that the insertion loss of the waveguides is reduced by on average 2.23 ± 1.2 dB after applying index matching fluid compared with the untreated case whereas the insertion loss was reduced on average by 2.60 dB ± 1.3 dB after applying the waveguide core polymer and curing it as described. Moreover, every waveguide had less loss with the new method compared to index matching fluid so the method is consistent and works correctly for many different lengths and types of waveguide having different numbers of bends and crossings which affect the modes present in the waveguide. In conclusion, the core polymer results in even more improvement than the index matching fluid and is far more robust as it is solid and does not evaporate nor collect dust. The 0.37 dB improvement over index matching fluid may be that the closest available index matching fluid differed by a possible 0.9% in refractive index from the core polymer refractive index, whereas using the core polymer itself produced a perfect match. No adverse effects were noticed due to the thin layer of core polymer over the surrounding cladding polymer. The error bars in Fig. 16 for both the index matching fluid and core polymer were very small in all cases showing an improvement in loss reproducibility across samples which is important in a manufacturing environment.

V. Conclusion

In this paper, detailed characterisation studies of the end facet roughness of polymer waveguides suitable for use in board-level optical interconnects are presented and a novel method of reducing the related optical coupling losses is proposed. The paper addresses some of the practical issues related to the adoption of this technology in real-world systems. The end facet roughness of multimode polyacrylate waveguides fabricated on FR4 PCBs, when cut at right angles to their optical axis by milling routers for optical butt-coupling connectors is compared with that resulting from dicing saws and polishing. The RMS surface roughnesses of polyacrylate waveguide end facets on FR4 PCB, due to milling routing at a range of rotation speeds and translation speeds are compared. One-flute routers gave significantly less rough surfaces than two or three-flute routers. The best results were achieved for a one-flute router when the milling bit was inserted from the PCB side of the board and the research optimized the milling parameters to minimize the optical loss. For the first time, to our knowledge, the waveguide optical insertion loss is shown to be linearly proportional to the ratio of the waveguide core end facet RMS roughness to its autocorrelation length. A new fabrication technique giving a more robust end facet for use in commercial products is proposed and demonstrated which reduces the insertion loss.

Acknowledgment

The authors are most grateful to Himanshu Suyal of Heriot Watt University for advice on release agents and curing polymer using UV light through microscope slides. The authors thank Xyratex, NPL, EPSRC, IeMRC, Dorothy Hodgkin Postgraduate awards and Stevenage Circuits Ltd for their financial and industrial support during this project. Also thanks to Ioannis

Papakonstantinou for help in polishing and copper removal from PCB and Steve Hudziak for use of the Nanotechnology laboratory and help with the AFM.

REFERENCES

[1] D. Miller, "Rationale and challenges for optical interconnects to electronic chips," *Proc. IEEE*, vol. 88, no. 6, pp. 728–749, 2000.

[2] H. Sung-Hwan, C. Mu-Hee, K. Sae-Kyoung, P. Hyo-Hoon, S. C. Han, K. Sang-Hoon, S. Kyoung-Up, and H. Sang-Won, "Passively assembled optical interconnection system based on an optical printed-circuit board," *IEEE Photon. Technol. Lett.*, vol. 18, no. 5, pp. 652–654, Mar. 2006.

[3] D. R. Selviah, D. A. Hutt, A. C. Walker, K. Wang, F. A. Fernandez, P. P. Conway, D. Milward, I. Papakonstantinou, H. Baghsiahi, J. Chappell, S. S. Zakariyah, A. McCarthy, and H. Suyal, "Innovative optical and electronic interconnect printed circuit board manufacturing research," in *Proc. 2nd Electron. Syst. Integration Technol. Conf., ESTC 2008*, 2008, pp. 867–872.

[4] R. Dangel, C. Berger, R. Beyeler, L. Dellmann, M. Gmur, R. Hamelin, F. Horst, T. Lamprecht, T. Morf, and S. Oggioni, "Polymer-waveguide-based board-level optical interconnect technology for datacom applications," *IEEE Trans. Adv. Packag.*, vol. 31, no. 4, pp. 759–767, 2008.

[5] R. Pitwon, K. Wang, J. Graham-Jones, I. Papakonstantinou, H. Baghsiahi, B. Offrein, R. Dangel, D. Milward, and D. Selviah, "Firstlight: Pluggable optical interconnect technologies for polymeric electro-optical printed circuit boards in data centers," *J. Lightw. Technol.*, vol. 30, no. 21, pp. 3316–3329, Nov. 2012.

[6] I. Papakonstantinou, D. R. Selviah, R. C. A. Pitwon, and D. Milward, "Low-cost, precision, self-alignment technique for coupling laser and photodiode arrays to polymer waveguide arrays on multilayer PCBs," *IEEE Trans. Adv. Packag.*, vol. 31, no. 3, pp. 502–511, 2008.

[7] J. Beals, IV, N. Bamiedakis, A. Wonfor, R. V. Penty, I. H. White, J. V. , Jr, T. V. Clapp, and M. Glick, "Terabit capacity passive polymer optical backplane," in *Conf. Lasers and Electro-Optics, Optical Soc. of Amer.*, 2008.

[8] S. S. Zakariyah, P. P. Conway, D. A. Hutt, D. R. Selviah, K. Wang, H. Baghsiahi, J. Rygate, J. Calver, and W. Kandulski, "Polymer optical waveguide fabrication using laser ablation," in *Proc. 11th Electron. Packaging Technol. Conf.*, 2009, pp. 936–941.

[9] S. S. Zakariyah, P. P. Conway, D. A. Hutt, D. R. Selviah, K. Wang, J. Rygate, J. Calver, and W. Kandulski, "Fabrication of polymer waveguides by laser ablation using a 355 nm wavelength Nd:YAG laser," *J. Lightw. Technol.*, vol. 29, no. 23, pp. 3566–3576, 2011.

[10] M. Komatsu, "Machining performance of a router bit in the peripheral milling of wood . effects of the helix angle of the peripheral cutting-edge on the cutting force and machined-surface roughness," *Mokuzai Gakkaishi*, vol. 40, no. 2, pp. 134–141, 1994.

[11] H. Kamata and T. Kanauchi, "Analysis of machined surfaces with distal image-processing .1. Effect of grain angle in numerical control router machining," *Mokuzai Gakkaishi*, vol. 39, no. 11, pp. 1253–1258, 1993.

[12] M. E. Teitelbaum, R. Nair, D. J. O'Brien, E. D. Wetzel, and K. W. Goossen, "Cost-effective integration of plastic optical fiber and total internal reflection mirrors in printed circuit boards for parallel optical interconnects," *Opt. Eng.*, vol. 49, no. 6, pp. 456–461, 2010.

[13] F. Morichetti, "Roughness induced backscattering in optical silicon waveguides," *Phys. Rev. Lett.*, vol. 104, no. 3, Jan. 2010.

[14] J. Nakayama, "Reflection, diffraction and scattering at low grazing angle of incidence: Regular and random systems," *IEICE Trans. Electron.*, vol. E94C, no. 1, pp. 2–9, 2011.

[15] G. M. Gallatin, "Resist blur and line edge roughness," *SPIE Optical Microlithogr.*, vol. 5754, pp. 38–52, May 2005.

[16] D. Maystre, "Rigorous theory of light scattering from rough surfaces," *Optics*, vol. 15, no. 1, pp. 43–51, 1984.

[17] J. M. Sotocrespo and M. Nietovesperinas, "Electromagnetic scattering from very rough random surfaces and deep reflection gratings," *J. Optical Soc. Amer. A—Optics Image Sci. Vision*, vol. 6, no. 3, pp. 367–384, 1989.

[18] M. Raposo, Q. Ferreira, and P. Ribera, "A Guide for Atomic Force Microscopy Analysis of Soft-Condensed Matter Research and Education Topics in Microscopy," 2007, pp. 758–769 [Online]. Available: http://www.formatex.org/microscopy3/pdf/

[19] Vortex Tool Ltd, Chip Load Chart and Information , 2011 [Online]. Available: http://www.vortextool.com/images/chipLoadChart.pdf

[20] I. Papakonstantinou, K. Wang, D. R. Selviah, and F. A. Fernandez, "Transition, radiation and propagation loss in polymer multimode waveguide bends," *Opt. Expr.*, vol. 15, no. 2, pp. 669–679, 2007.

Hadi Baghsiahi (M'09) received the Bachelor degree in physics from Shiraz University, Iran, in 2002 and the M.Sc. degree in Photonics and Optical Telecommunications from Shahid Bahonar University of Kerman, in 2005. He received the Ph.D. degree from University College London in 2012 for research on optical printed circuit boards, OPCBs. He is also researching into designs of light engine for laser based 3D autostereoscopic displays.

Kai Wang (M'02) received the B.Sc. degree in Electronic Engineering and Telecommunications from Shenzhen University, China, in 2001, and the M.Sc. degree in Microelectronic Systems and Telecommunications from Liverpool University in 2002. In 2003, he began Ph.D. research in the Department of Electronic and Electrical Engineering, University College London (UCL), becoming a research fellow in 2004. His current research includes computer modeling in LCDs, backlights, multimode waveguides and design OPCBs.

Witold Kandulski received the M.Sc.-Eng. in Technical Physics at Poznan University of Technology, Poland. He then became a research scientist at the Centre of Advanced European Study and Research in Bonn, focused on nanolithography, magnetic nanoparticles and metamaterials. For this work he received his Ph.D. in experimental physics at Rheinische Friedrich-Wilhelms-Universität, Bonn. He joined Stevenage Circuits Ltd and focused on PCB engineering, improvement of manufacturing methods for medical products and R&D of OPCBs. Currently based at UTC Aerospace Systems he is working on NPI of motor drive control systems. His interests include manufacturing, materials, engineering, nanotechnology and microscopy.

Richard C. A. Pitwon received his first degree (BSc Hons) in Physics from the University of St Andrews in 2000. He currently serves as Lead Photonics Engineer at Xyratex with over 12 years experience in the design and development of high speed photonic interconnect technologies including passive and active optical connectors, optical printed circuit boards, optical interconnect interfaces and transceivers. He holds 21 patents in the field of embedded optical interconnect and has authored numerous conference, journal and commercial publications in this area. He is a Chartered engineer (CEng) with the IET and represents the UK on International Electrotechnical Commission (IEC) optical interconnect standards committees.

David R. Selviah (M'01) received the M.A. degree in physics and theoretical physics and the Ph.D. degree in photonic engineering from Trinity College, Cambridge University, Cambridge, U.K. He is Chartered Physicist, Chartered Scientist and Reader in Optical Devices, Interconnects, Algorithms and Systems at Department of Electronic and Electrical Engineering, UCL (University College London), London, U.K., has over 200 publications, patents, book chapters, invited and plenary presentations led the £1.6 million IeMRC Optical Printed Circuit Board Flagship Consortium of 3 universities and 8 companies, and serves on International Electrotechnical Commission (IEC) standards committees.